RSC Advances

ROYAL SOCIETY OF CHEMISTRY

www.rsc.org/advances

Carbon supported Pt-Sn/SnO_2 anode catalyst for direct ethanol fuel cells

S. Meenakshi, P. Sridhar* and S. Pitchumani

Binary Pt-Sn/SnO_2-C electro-catalysts comprising Pt and Sn in varying weight ratio, namely 31:9, 33:7 and 35:5, were synthesized by an alcohol-reduction process using ethylene glycol as solvent and reducing agent. The electro-catalysts were characterized by XRD, XPS, TEM, SEM-EDAX, ICP-OES, Cyclic Voltammetry (CV), Chronoamperometry and CO stripping techniques. XRD spectra reveal shifting of Pt diffraction peaks to lower angles with the addition of Sn compared with Pt-C and also the presence of SnO_2. XPS results also confirm the presence of Sn in the form of PtSn alloy and in the form of SnO_2 phase in the catalyst. The effect of composition towards electro-oxidation of ethanol has been studied by CV technique. The direct ethanol fuel cells (DEFCs) with Pt-Sn/SnO_2-C anode catalyst with reduced Pt loading exhibits an enhanced peak power density of 27.0 mW cm^{-2} while a peak power-density of only 2.2 mW cm^{-2} is obtained for the DEFC employing Pt-C at 90 ^oC.

CSIR-Central Electro Chemical Research Institute-Madras Unit, CSIR Madras Complex, Taramani, Chennai 600 113, India.

E-mail address: psridhar@csircmc.res.in; Tel.: +91 44 2254 4554; Fax: +91 44 2254 2456

Introduction

Low temperature polymer electrolyte fuel cells (PEFCs) fueled directly by liquid fuels are gaining attention. Operation on liquid fuels without the external bulky fuel-reforming system could greatly simplify the fuel cell system.[1] At present methanol has been considered the most promising fuel because it is more efficiently oxidized than other alcohols. However, methanol is a toxic compound and its use on a large scale can cause some environmental and safety problems.[2] On the other hand, as an alternative fuel ethanol is safer and compared with methanol (6.1 kWh kg^{-1}), ethanol has higher energy density (8.2 kWh kg^{-1}). In addition, it can be produced in large quantities from biomass through fermentation process of renewable resources such as sugarcane, wheat, corn or straw. However, its complete oxidation to CO_2 is difficult since ethanol has strong C-C bond in the molecule.[3-5]

Many studies have investigated the carbon supported Pt as an anode catalyst for low temperature fuel cells. But Pt itself is rapidly poisoned on its surface by ethanol oxidation. Therefore, most of the researchers concentrated on binary and ternary metal based catalyst. For the binary system Pt-Ru/C,[6] Pt-Sn/C,[7-14] Pt-W/C,[15] Pt-Pd/C,[16] Pt-Re/C,[17] Pt-Rh/C,[18] Pt-Mo/C,[19] Pt-CeO_2/C,[20] Pt-ZrO_2/C,[21] Pt-RuO_2/C,[22] TNT/Pt/C[23] and Pt_x-WO_3/C[24] were used as anode catalysts. Among these, Pt-Sn based binary system is the most active electro-catalyst for ethanol electro-oxidation. Pt-Sn alloy and Pt-SnO_2/C,[25,26] carbon supported $Pt_{75}Sn_{25}$,[27] decoration of carbon supported Pt with Sn,[28] alloy Pt_7Sn_3 and bi-phase Pt-SnO_x nano-catalyst[29] were some of the catalysts that have been studied. Higuchi *et al.*[30] reported highly dispersed Pt-SnO_2 nanoparticle on carbon black. Zhu *et al.*[31] have reported on the effect of alloying degree in PtSn catalyst, SnO_2@Pt/C[5] and also the enhanced ethanol oxidation reaction (EOR) activity of carbon

supported Pt50Sn50 alloy catalyst.[32] There are two different schools of thought on the enhanced activity for EOR while using Pt-Sn as an anode catalyst. One group attributes this to Pt-Sn in the alloy form while another group favours Pt-Sn as a binary mixture or Sn present in the form of SnO_2. Antolini *et al.*[33] investigated the effect of the alloy phase characteristics on carbon supported (PtSn)alloy/SnO_2 and (PtSnPd)alloy/SnO_2 catalyst. In order to enhance the fuel cell performance further they had introduced a third metal to the catalyst but not with success.

The present study is focused on the requirement of oxidation state of Sn in carbon supported Pt-Sn catalyst for ethanol oxidation. Pt-Sn/SnO_2-C (Pt: Sn in weight ratio of 31:9, 33:7 and 35:5) and Pt-C electrocatalysts were prepared using ethylene glycol as the reducing agent. In the catalyst, Pt-Sn/SnO_2-C, Sn is present in the form of SnO_2 as well as alloyed with Pt. Presence of Sn in alloy as well as SnO_2 form in the catalysts were established using XRD and XPS techniques. Cyclic Voltammetry (CV), Chronoamperometry (CA) and CO stripping experiments were carried out to study the effect of the catalytic activity of Sn present in the catalyst. Direct ethanol fuel cell (DEFC) single cell performance was also studied.

Experimental

Materials

All chemicals were analytically pure and used as received. The precursors dihydrogen hexachloroplatinate (IV) hexahydrate ($H_2PtCl_6.6H_2O$) was procured from Johnson Matthey Chemicals India Pvt. Ltd and Tin chloride ($SnCl_2$), anhydrous (98%) was obtained from Alfa Aesar. Vulcan XC-72 carbon was procured from Cabot Corp. 5wt% Nafion ionomer was received from DuPont. Ethanol (CH_3CH_2OH), 2-Propanol and ethylene glycol were obtained

from Merck-India and Perchloric acid ($HClO_4$) from Rankem-India. De-ionized water (18 MΩ cm) was used during the study.

Preparation of carbon supported Pt-Sn/SnO_2 composite catalysts

Pt-Sn (40 wt%)/C catalyst was synthesized by alcohol reduction process. In brief, calculated amount of the precursors $H_2PtCl_6.6H_2O$ and $SnCl_2$ and the support, Vulcan XC -72 carbon, were dispersed with ethylene glycol using ultrasonicator for a few minutes and followed by stirring kept for 1 h. Then the above resultant solution was mixed with the precursors followed by support under stirring condition for 2 h. After that aqueous solution of 0.05 M NaOH was added to adjust the alkaline pH. The obtained mixture was refluxed for 5 h at 130 ^oC. The product was collected by filtration and washed well with copious DI water, then dried at 80 ^oC for 24 h. Pt-Sn/C composite catalysts containing Pt and Sn in varying atomic ratios, namely 2:1, 3:1 and 4:1 were prepared. Carbon-supported Pt was also prepared by the same procedure for comparison. In all the prepared Pt-Sn/C catalyst, along with the elemental form, presence of the oxide form of Sn was also identified with the help of XRD. For convenience, the prepared catalysts were named on the basis of weight ratios between Pt and Sn obtained from the preparation procedure as 31:9, 33:7 and 35:5.

Physical characterization of the catalysts

XRD patterns of all the catalysts were obtained on a BRUKER-binary V3 diffractometer using Cu K_α radiation (λ =1.5406 Å) between 10 and 80° in reflection geometry in steps of 5° min^{-1}. The crystallite size was calculated using Scherrer formula. The structure and distribution of electro-catalysts were examined under a 200 kV Tecnai-20 G2 transmission electron microscope

(TEM). The samples were suspended in acetone with ultrasonic dispersion for 3 min. Subsequently, a drop of the suspension was deposited on a holey carbon grid followed by drying. TEM images for the samples were recorded with a Multiscan CCD Camera (Model 794, Gatan) using low-dose condition. Surface scanning electron micrographs and Energy dispersive analysis by X-rays (EDAX) for electro-catalysts were obtained using JEOL JSM 35CF Scanning Electron Microscope (SEM). X-ray photoelectron spectroscopy (XPS, Thermo Fisher Scientific, ESCALAB 250 XPS system) using monochromatic Al K_α source at 15 keV and 150 W system was used to identify the interaction of Sn with Pt. ICP-OES was used to analyze the bulk composition of Pt to Sn in Pt-Sn/SnO_2(31:9)-C, Pt-Sn/SnO_2(33:7)-C and Pt-Sn/SnO_2(35:5)-C catalysts. For this purpose, the catalyst was dissolved in concentrated aqua regia followed by dilution with water to concentrations ranging between 1 and 50 ppm as desired for the analysis. The actual composition was determined from the calibration curves of known standards.

Electrochemical characterization of the catalysts

CV experiments were carried out by employing Biologic science instruments (VSP) utilizing the EC-Lab software. A glassy carbon (GC) disk with a geometrical area of 0.071 cm^2 as a working electrode, saturated calomel electrode (SCE) and Pt foil were used as reference and counter electrodes, respectively. The working electrodes were prepared using an ink made of catalyst materials. 10 μL aliquot of the dispersion was pipetted onto the GC. After evaporation of water, 5 μL of a diluted Nafion solution (0.05 M) was pipetted onto the electrode surface to attach the catalyst particles onto the GC. The electrode was dried at room temperature. Prior to any electrochemical measurement, the working electrode was cycled several times between -0.25 and 0.8 V with respect to SCE at a sweep rate of 50 mV s^{-1} to activate the electrode until a stable

curve was obtained. Chronoamperometry (CA) curves were recorded at 0.3 V and 0.5 V holding the electrode at the same potential for 1800 s. CV and CA were performed in solutions containing 0.5 M $HClO_4$ and 1.0 M ethanol saturated with N_2. CO stripping voltammetry was conducted for the Pt-Sn/SnO_2(33:7)-C catalyst. 0.5 M $HClO_4$ was used as an electrolyte, in the first step CO was adsorbed on the electrode at 0.1 V for 30 min. After that, the electrolyte was purged with N_2 for 10 min to remove excess of CO from the electrolyte holding the potential at 0.1 V. Then, the stripping was performed between 0.2 and 0.7 V with respect to SCE at a sweep rate of 10 mV s^{-1}.

Preparation of membrane-electrode assemblies and their performance evaluation

Membrane electrode assemblies (MEAs) were tested using 4 cm^2 single cell set up. The fabrication of MEA was described elsewhere.[34] In brief, 15 wt% teflonized Toray TGP-H-120 carbon paper of 0.37 mm thick was used as the backing layer. To prepare a gas diffusion layer (GDL), Vulcan XC-72R carbon was suspended in cyclohexane and agitated in an ultrasonic water bath for 30 min. To this solution, 15 wt% poly(tetrafluroethene) (PTFE) suspension in 2 mL ammonia was added with continuous agitation to form a slurry to coat on the backing layer uniformly until the required loading of 1.5 mg cm^{-2} was attained. The GDL thus obtained was sintered in a furnace at 350 °C for 30 min. K-Coater was used to make electrodes. Catalyst ink comprised the required amount of prepared Pt-C or commercial Pt-C or Pt-Sn/SnO_2(33:7)-C, H_2O, ethanol, propylene glycol and Nafion solution. 120 μ bar rod was used for coating the anode catalyst layer with a loading of 0.2 mg cm^{-2} while 150 μ bar rod was used for cathode catalyst layer with a loading of 0.35 mg cm^{-2}. Totally four transfers were effected on each side of the membrane, the initial transfer at 130 ^oC without any pressure for 2 min and subsequent

transfers at 20 kg cm^{-2} for 5 min. Then the GDL was pressed over the catalyst layer. Total catalyst loadings for anode and cathode after all the transfers were 0.75 mg cm^{-2} and 1.25 mg cm^{-2}, respectively. MEAs were evaluated using a fuel cell fixture with parallel serpentine flow-field machined on graphite plates. The cell was tested at 70, 80 and 90 ^{o}C with 2 M aq. ethanol at a flow rate of 2 mL min^{-1} at the anode and oxygen at a flow rate of 300 mL min^{-1} at atmospheric pressure at the cathode. Measurements for cell potentials with varying current densities were conducted galvanostatically using Model-LCN4-25-24/LCN 50-24 procured from Bitrode Instruments (US).

Results and discussion

XRD analysis for the catalysts

The XRD patterns of the as prepared Pt-Sn/SnO_2-C and Pt-C catalysts are shown in Fig. 1. A broad peak at about 25^{o} is associated with the carbon material and peaks at 39.7^{o}, 46.2^{o}, 67.6^{o} are associated with the (1 1 1), (2 0 0) and (2 2 0) crystalline planes of Pt, respectively. These diffraction peaks are shifted to lower 2θ values for Pt-Sn/SnO_2-C catalysts in relation to Pt-C. It is clear from Fig. 2, the diffraction peaks for Pt in Pt-Sn are shifted to 2θ values of 66.43^{o} compared to 67.58^{o} for Pt in Pt-C as shown distinctly for (2 2 0) crystalline plane. The observed shift in peak for this plane is due to the alloy formation in the catalyst. In the diffraction pattern two more peaks observed at 33.8^{o} and 52^{o} represent crystalline planes (1 0 1) and (2 1 1), respectively of SnO_2 as shown in inset of Fig. 2. It clearly shows that Sn is also present in the form of SnO_2 in the catalyst. Crystallite sizes of the catalysts are calculated from Pt (1 1 1) crystalline plane using Scherrer formula. The results are listed in Table 1.

TEM and SEM analyses for the catalysts

Fig. 3 presents the TEM images of Pt-Sn/SnO_2(31:9)-C, Pt-Sn/SnO_2(33:7)-C, Pt-Sn/SnO_2(35:5)-C and Pt-C electro-catalysts. It can be seen clearly that all the catalysts have a smaller particle size and uniform particle size distribution in the catalyst matrix. The mean particle sizes of Pt-Sn/SnO_2(31:9)-C, Pt-Sn/SnO_2(33:7)-C, Pt-Sn/SnO_2(35:5)-C and Pt-C are presented in Table 1. These results indicate that ethylene glycol synthesis method for preparation of catalyst has resulted in the formation of homogeneous and small particles on carbon. From the SEM micrograph in Fig. 4, it is clear that the Pt-Sn particles are uniformly dispersed on the carbon surface and the incorporation of Sn in the catalyst support is confirmed as seen in the typical image (Fig. 4(b)) given for Pt-Sn/SnO_2(33:7)-C catalyst. ICP-OES analysis was performed for a Pt-Sn/SnO_2(31:9)-C, Pt-Sn/SnO_2(33:7)-C and Pt-Sn/SnO_2(35:5)-C catalyst and the result is given in Table 1. The data suggest that the surface composition of the catalyst is similar to that in the bulk.

XPS analysis of the catalyst

XPS is a useful technique to analyze the surface oxidation states in the catalyst. Pt(4f) spectra for Pt-C and Pt-Sn/SnO_2(33:7)-C catalysts are shown in Fig. 5a and Fig. 5b, respectively. Spectra exhibited intense doublets that are assigned to Pt($4f_{7/2}$) and Pt($4f_{5/2}$) at 71.62 and 74.84 eV for Pt-C catalyst and at 71.94 and 75.12 eV for Pt-Sn/SnO_2(33:7)-C catalyst, respectively. It is clear that peak binding energies of Pt($4f_{7/2}$) and Pt($4f_{5/2}$) slightly shifted to higher binding energies (0.32 and 0.28 eV) for Pt-Sn/SnO_2(33:7)-C catalyst[35], which may be due to the charge transfer from Sn to Pt because of the lower electronegativity of Sn (1.8) in relation to Pt (2.2).[36] The charge transfer from Sn atoms to Pt atoms increases the electron density around the Pt sites,

which leads to weakened chemisorption energy with oxygen containing species. This modification of the electronic environment around Pt-sites enhances the electrocatalytic activity of the catalyst. Fig. 5c indicates that Sn(3d) spectra exhibited intense doublets assigned to $3d_{3/2}$ and $3d_{5/2}$ at 495.7 and 487.3 eV, respectively corresponding to the binding energies of Sn(IV) in SnO_2[28,37] and also confirms that Sn is present in the elemental Sn(0) form based on the binding energy at 485.70 eV.[31] Sn in the oxide form will give an additional advantage of synergistic effect arising from the combination of Pt and SnO_2 through the bifunctional mechanism as suggested by Higuchi *et al.*[30] SnO_2 in the Pt-Sn/SnO_2-C catalyst helps in enhancing the ethanol oxidation by lowering the oxidation potential of Pt-adsorbed CO via a bifunctional mechanism.[30,31]

Cyclic voltammetry in 0.5 M $HClO_4$

Fig. 6 exhibits cyclic voltammograms of Pt-Sn/SnO_2(31:9)-C, Pt-Sn/SnO_2(33:7)-C, Pt-Sn/SnO_2(35:5)-C and Pt-C electro-catalyst in 0.5 M aq. $HClO_4$ at a scan rate of 50 mV s^{-1}. H_2 adsorption/desorption between 0 and 0.3 V (vs. NHE) followed by the "double-layer" potential region and above 0.7 V (vs. NHE) oxide formation/reduction regions are observed. The voltammograms demonstrate the H_2 adsorption/desorption between 0 and 0.3 V (vs. NHE) for all the catalysts. It clearly shows that Pt-Sn based catalysts have a higher distinct H_2 adsorption/desorption region and the peaks are also shifted to lower potential in relation to Pt-C. Larger capacitive current observed in the double layer region for Pt-Sn/SnO_2(33:7)-C catalyst may be due to higher segregation of SnO_2 species in comparison to Pt-Sn/SnO_2 (35:5)-C and Pt-Sn/SnO_2(31:9)-C catalysts.[5,30] Inset of Fig. 6 shows the voltammograms of oxide formation/reduction regions between 0.5 and 1.0 V for Pt-C and Pt-Sn/SnO_2(33:7)-C catalysts,

therein small peaks appear at around 0.59 and 0.71 V, which may be assigned to the adsorption and desorption of oxygen-containing species resulting from the dissociation of water on SnO_2.[13] The electrochemical active surface area (ESA) was calculated using the H_2 desorption peak area of the CV curves. The ESA can be calculated from the following equation:[38]

$$\text{ESA } (\text{cm}^2\ \text{g}^{-1}{}_{\text{Pt}}) = \frac{Q_H\left(\mu\text{C}\ \ \text{cm}^{-2}\right)}{210\,\mu\text{C}\ \ \text{cm}^{-2} \times \text{electrode}\ \ \text{loading}\left(g_{\text{Pt}}\ \ \text{cm}^{-2}\right)} \quad (1)$$

where Q_H represents the charge of hydrogen desorption and 210 μC cm^{-2} is the charge required to oxidize a monolayer of H_2 on smooth platinum surface. The estimated ESA values of all the catalysts are given in Table 2. Pt-Sn/SnO_2(33:7)-C shows higher ESA compared with all the other catalysts. The improved ESA is due to the quick adsorption and easy desorption of H_2 on the Sn modified Pt surface in relation to carbon supported pristine Pt in $HClO_4$ system.

Cyclic voltammetry in presence of ethanol

Fig. 7 shows cyclic voltammograms for electro-oxidation of ethanol on Pt-Sn/SnO_2(31:9)-C, Pt-Sn/SnO_2(33:7)-C, Pt-Sn/SnO_2(35:5)-C and Pt-C electro-catalysts in 0.5 M aq. $HClO_4$ and 1 M aq. CH_3CH_2OH at a scan rate of 50 mV s^{-1}. The onset potential shifted towards negative for Pt-Sn/SnO_2(33:7)-C catalyst compared to all the other catalysts; the lowest onset potential obtained for the oxidation of ethanol is due to an electronic effect and bifunctional effect in the Sn modified Pt-based materials. Mass activities are calculated for the above referred catalysts at 0.8 V and the results are given in Table 2. Pt-Sn/SnO_2(33:7)-C catalyst gives higher mass activity as compared to Pt-Sn/SnO_2(31:9)-C, Pt-Sn/SnO_2(35:5)-C and Pt-C catalysts.

CO stripping and Chronoamperometry studies for the catalysts

CO species are the main poisoning intermediates during ethanol electro-oxidation.[23] An effective catalyst should have excellent CO electro-oxidation ability, which can be ascertained by CO stripping experiment. Fig. 8 shows CO stripping curves for Pt-C and Pt-Sn/SnO_2(33:7)-C catalysts obtained at a sweep rate of 10 mV s^{-1} in $HClO_4$ electrolyte at room temperature. The onset potentials for CO oxidation are around 620 and 330 mV while the peak potentials are at 680 and 635 mV (vs. NHE) for Pt-C and Pt-Sn/SnO_2(33:7)-C catalysts, respectively. The potential shifted negative for Pt-Sn catalyst in relation with Pt-C, which is in agreement with literature.[39,40] The negative shift in potential in the stripping voltammogram for the catalyst is due to the presence of oxygenated species on Sn sites formed at lower potentials in comparison with Pt. According to bifunctional mechanism, these oxygenated species allow the oxidation of CO to CO_2 at lower potentials. Vigier *et al.*[40] accounted that SnO_2 could supply the oxygen species for the oxidation of CO adsorbed on the Pt sites, thereby enhancing the oxidation of ethanol at lower potentials. Furthermore, the shape of the CO stripping peak depends on the nature of the catalyst, the range of potential allowing for oxidation of CO on the Pt-Sn/SnO_2(33:7)-C catalyst is wider than Pt-C. This confirms that SnO_2 enhances the catalytic activity of Pt-Sn/SnO_2(33:7)-C catalyst. The chronoamperometry experiments are performed to study the electrochemical stability of the electro-catalysts. Fig. 9(a-c) presents the chronoamperometric curves for the prepared Pt-C, commercial Pt-C and Pt-Sn/SnO_2(33:7)-C catalysts at 0.5 and 0.3 V (vs. NHE). Currents are normalized for Pt loading and plotted against time. It can be clearly seen that the current dropped rapidly at first and then became relatively stable. The mass activities under steady state condition for ethanol oxidation on commercial Pt-C, prepared Pt-C and Pt-Sn/SnO_2(33:7)-C are 13, 12, 123 mA mg^{-1}_{Pt} at 0.5 V and 1.2, 1.1, 17.0

mA mg^{-1}_{Pt} at 0.3 V, respectively. It is interesting to note that the mass activity is higher for Pt-Sn/SnO_2(33:7)-C catalyst than the prepared and commercial Pt-C and also than that reported for Pt-Sn/C catalyst.[5] The higher activity obtained is due to the fact that SnO_2 can transform CO-like poisoning species on Pt into CO_2, leaving the active sites on Pt for further adsorption and oxidation of ethanol by the bifunctional mechanism.[41]

Performance evaluation for DEFCs

Single cell DEFC performances are examined for Pt-Sn/SnO_2-C anode catalyst. Fig. 10(a-c) shows the performance for commercial Pt-C, prepared Pt-C and Pt-Sn/SnO_2(33:7)-C catalyst (chosen based on half-cell studies) at 70, 80 and 90 ^oC. Peak power densities of 2.6, 2.2 and 27.0 mW cm^{-2} are obtained for MEAs comprising commercial Pt-C, prepared Pt-C and Pt-Sn/SnO_2(33:7)-C catalysts respectively, at 90 ^oC under ambient pressure. Pt-Sn/SnO_2-C as anode catalyst exhibited enhanced peak power density with reduced loading of 0.75 mg cm^{-2} compared with Pt-C and also that reported in the literature with a higher loading of 2.0 mg cm^{-2}.[2,27,42,43]

Conclusions

Carbon supported Pt-Sn/SnO_2 catalysts were synthesized by alcohol-reduction method. XRD and XPS measurements confirm the presence of Sn both in alloy form with Pt and in the form of oxide. Electrochemical characterization reveals excellent EOR activity for Pt-Sn/SnO_2(33:7)-C catalyst. Single cell performance of DEFC with Pt-Sn/SnO_2(33:7)-C as anode catalyst shows an enhanced peak power density of 27 mW cm^{-2} at 90 ^oC. It is interesting to note that this performance is superior to that reported in the literature with a higher loading of Pt to the extent of 2.0 mg cm^{-2}. The combined effect of weakened chemisorption of oxygen due to the interactive

nature of Pt-Sn alloy and the ability of SnO_2 in transforming CO-like poisoning species on Pt into CO_2 has made Pt-Sn/SnO_2-C catalyst as a superior anode catalyst for ethanol electro-oxidation in direct ethanol fuel cells.

Acknowledgements

S. Meenakshi is grateful to CSIR, New Delhi, for a Senior Research Fellowship. The authors are thankful to Dr Vijaymohanan Pillai, Director, CSIR-CECRI for his encouragement and support.

References

1 W. J. Zhou, B. Zhou, W. Z. Li , Z. H. Zhou, S. Q. Song, G. Q. Sun, Q. Xin, S. Douvartzides, M. Goula and P. Tsiakaras, *J. Power Sources*, 2004, **126**, 16-22.

2 C. Lamy, S. Rousseau, E. M. Belgsir, C. Coutanceau and J. -M. Léger, *Electrochim. Acta*, 2004, **49**, 3901-3908.

3 E. Antolini, *J. Power Sources*, 2007, **170**, 1-12.

4 E. Antolini and E. R. Gonzalez, *Catal. Today*, 2011, **160**, 28-38.

5 J. C. M. Silva, R. F. B. De Souza, L. S. Parreira, E. Teixeira Neto, M. L. Calegaro and M. C. Santos, *Appl. Catal. B: Environ.*, 2010, **99**, 265-271.

6 H. Pramanik and S. Basu, *Can. J. Chem. Eng.,* 2007, **85**, 781-785.

7 M. Brandalise, M. M. Tusi, R. M. S. Rodrigues, E. V. Spinacé and A. O. Neto, *Int. J. Electrochem. Sci.,* 2010, **5**, 1879-1886.

8 S. C. Zignani, E. R. Gonzalez, V. Baglio, S. Siracusano and A. S. Aricò, *Int. J. Electrochem. Sci.,* 2012, **7**, 3155-3166.

9 L. Jiang, G. Sun, S. Sun, J. Liu, S. Tang, H. Li, B. Zhou and Q. Xin, *Electrochim. Acta*, 2005, **50**, 5384-5389.

10 B. Su, K. Wang, C. Tseng, C. Wang and Y. Hsueh, *Int. J. Electrochem. Sci.*, 2012, **7**, 5246 - 5255.

11 L. Jiang, G. Sun, Z. Zhou, W. Zhou and Q. Xin, *Catal. Today*, 2004, **93-95**, 665-670.

12 A. O. Neto, R. W. R. Verjulio-Silva, M. Linardi and E. V. Spinacé, *Ionics*, 2010, **16**, 85-89.

13 D.-H. Lim, D.-H. Choi, W.-D. Lee, D.-R. Park and H.-I. Lee, *Electrochem. Solid State Lett.*, 2007, **10**, B87-B90.

14 B. Liu, Z. -W. Chia, Z. -Y. Lee, C. -H. Cheng, J. -Y. Lee and Z. -L. Liu, *Fuel Cells*, 2012, **12**, 670-676.

15 S. Tanaka, M. Umeda, H. Ojima, Y. Usui, O. Kimura and I. Uchida, *J. Power Sources*, 2005, **152**, 34-39.

16 W. J. Zhou, W. Z. Li, S. Q. Song, Z. H. Zhou, L. H. Jiang, G. Q. Sun, Q. Xin, K. Poulianitis, S. Kontou and P. Tsiakaras, *J. Power Sources,* 2004, **131**, 217-223.

17 F. Vigier, C. Coutanceau, A. Perrard, E. M. Belgsir and C. Lamy, *J. Appl. Electrochem.,* 2004, **34**, 439-446.

18 S. S. Gupta and J. Datta, *J. Electroanal. Chem.,* 2006, **594**, 65-72.

19 D. M. dos Anjos, K. B. Kokoh, J.-M. Léger, A. R. DE Andrade, P. Olivi and G. Tremiliosi-Filho, *J. Appl. Electrochem.,* 2006, **36**, 1391-1397.

20 Y. Bai, J. Wu, X. Qiu, J. Xi, J. Wang, J. Li, W. Zhu and L. Chen, *Appl. Catal. B: Environ.*, 2007, **73**, 144-149.

21 Y. Bai, J. Wu, J. Xi, J. Wang, W. Zhu, L. Chen and X. Qiu, *Electrochem. Commun.*, 2005, **7**, 1087-1090.

22 M. L. Calegaro, H. B. Suffredini, S. A. S. Machado and L. A. Avaca, *J. Power Sources*, 2006, **156**, 300-305.

23 H. Song, X. Qiu, X. Li, F. Li, W. Zhu and L. Chen, *J. Power Sources* 2007, **170**, 50-54.

24 D. Zhang, Z. Ma, G. Wang, K. Konstantinov, X. Yuan and H. Liu, *Electrochem. Solid State Lett.*, 2006, **9**, A423-A426.

25 J. C. M. Silva, L. S. Parreira, R. F. B. De Souza, M. L. Calegaro, E. V. Spinacé, A. O. Neto and M. C. Santos, *Appl. Catal. B: Environ.*, 2011, **110**, 141-147.

26 L. Jiang, L. Colmenares, Z. Jusys, G. Q. Sun and R. J. Behm, *Electrochim. Acta*, 2007, **53**, 377-389.

27 F. Colmati, E. Antolini and E. R. Gonzalez, *Appl. Catal. B: Environ.*, 2007, **73**, 106-115.

28 G. Li and P. G. Pickup, *J. Power Sources*, 2007, **173**, 121-129.

29 E. A. Baranova, T. Amir, P. H. J. Mercier, B. Patarachao, D. Wang and Y. L. Page, *J. Appl. Electrochem.,* 2010, **40**, 1767-1777.

30 E. Higuchi, K. Miyata, T. Takase and H. Inoue, *J. Power Sources,* 2011, **196**, 1730-1737.

31 M. Zhu, G. Sun and Q. Xin, *Electrochim. Acta,* 2009, **54**, 1511-1518.

32 F. Colmati, E. Antolini and E. R. Gonzalez, *J. Solid State Electrochem.*, 2007, **12**, 591-599.

33 E. Antolini, F. Colmati and E. R. Gonzalez, *J. Power Sources*, 2009, **193**, 555-561.

34 S. Meenakshi, A. K. Sahu, S. D. Bhat, P. Sridhar, S. Pitchumani and A. K. Shukla, *Electrochim. Acta*, 2013, **89**, 35-44.

35 N. Murata, T. Suzuki, M. Kobayashi, F. Togoh and K. Asakura, *Phys. Chem. Chem. Phys.*, 2013, **15**, 17938-17946.

36 A. S. Aricò V. Antonucci, N. Giordano, A. K. Shukla, M. K. Ravikumar, A. Roy, S. R. Barman and D. D. Sarma, *J. Power Sources*, 1994, **50**, 295-309.

37 X. Li, B. Lin, B. Xu, Z. Chen, Q. Wang, J. Kuang and H. Zhu, *J. Mater. Chem.,* 2010, **20**, 3924-3931.

38 G. Selvarani, A. K. Sahu, N. A. Choudhury, P. Sridhar, S. Pitchumani and A. K. Shukla, *Electrochim. Acta*, 2007, **52**, 4871-4877.

39 F. Colmati, E. Antolini and E. R. Gonzalez, *J. Power Sources*, 2006, **157**, 98-103.

40 F. Vigier, C. Coutanceau, F. Hahn, E. M. E. M. Belgsir and C. Lamy, *J. Electroanal. Chem.,* 2004, **563**, 81-89.

41 H. Li, D. Kang, H. Wang and R. Wang, *Int. J. Electrochem.* Sci., 2011, **6**, 1058-1065.

42 S. Rousseau, C. Coutanceau, C. Lamy and J. –M. Léger, *J. Power Sources*, 2006, **158**, 18-24.

43 C. Lamy, C. Coutanceau and J.–M. Léger, Catalysis for Sustainable Energy Production, (Eds.) by P. Barbaro and C. Bianchini, Wiley-VCH Verlag Gmbh and Co. KGaA, 2009, Weinheim.

Figure captions

Fig. 1 Powder XRD patterns for (a) Pt-C, (b) Pt-Sn/SnO_2(31:9)-C, (c) Pt-Sn/SnO_2(33:7)-C and (d) Pt-Sn/SnO_2(35:5)-C catalysts.

Fig. 2 Powder XRD patterns and inset for (a) Pt-C and (b) Pt-Sn/SnO_2(33:7)-C catalysts.

Fig. 3 Transmission electron micrographs for (a) Pt-C, (b) Pt-Sn/SnO_2(31:9)-C, (c) Pt-Sn/SnO_2(33:7)-C and (d) Pt-Sn/SnO_2(35:5)-C catalysts.

Fig. 4 (a) SEM micrographs and (b) EDAX image for Pt-Sn/SnO_2(33:7)-C catalyst.

Fig. 5 X-ray photoelectron spectra for (a) Pt-C, (b) and (c) Pt-Sn/SnO_2(33:7)-C catalysts.

Fig. 6 Cyclic voltammograms for Pt-Sn/SnO_2(31:9)-C, Pt-Sn/SnO_2(33:7)-C, Pt-Sn/SnO_2(35:5)-C and Pt-C catalysts containing Pt and Sn in varying weight ratios and inset shows the voltammogram of oxide formation/reduction regions of (a) Pt-C and (b) Pt-Sn/SnO_2(33:7)-C catalysts in N_2-saturated aq. 0.5 M $HClO_4$ at a scan rate of 50 mV s^{-1}.

Fig. 7 Cyclic voltammograms for Pt-Sn/SnO_2(31:9)-C, Pt-Sn/SnO_2(33:7)-C, Pt-Sn/SnO_2(35:5)-C and Pt-C catalysts containing Pt and Sn in varying weight ratios in aq. solution containing 0.5 M $HClO_4$ and 1 M CH_3CH_2OH saturated with N_2 at a scan rate of 50 mV s^{-1}.

Fig. 8 Stripping voltammograms of adsorbed CO on Pt-C and Pt-Sn/SnO_2(33:7)-C electrocatalysts recorded at 10 mV s^{-1}.

Fig. 9 Current vs. time dependence measured by chronoamperometry method in aq. solution containing 0.5 M $HClO_4$ and 1 M CH_3CH_2OH on (a) commercial Pt-C, (b) prepared Pt-C and (c) Pt-Sn/SnO_2(33:7)-C catalysts.

Fig. 10 Steady-state performance data of DEFCs (CH_3CH_2OH and O_2) comprising MEAs with (a) commercial Pt-C, (b) prepared Pt-C and (c) Pt-Sn/SnO_2(33:7)-C anode catalysts.

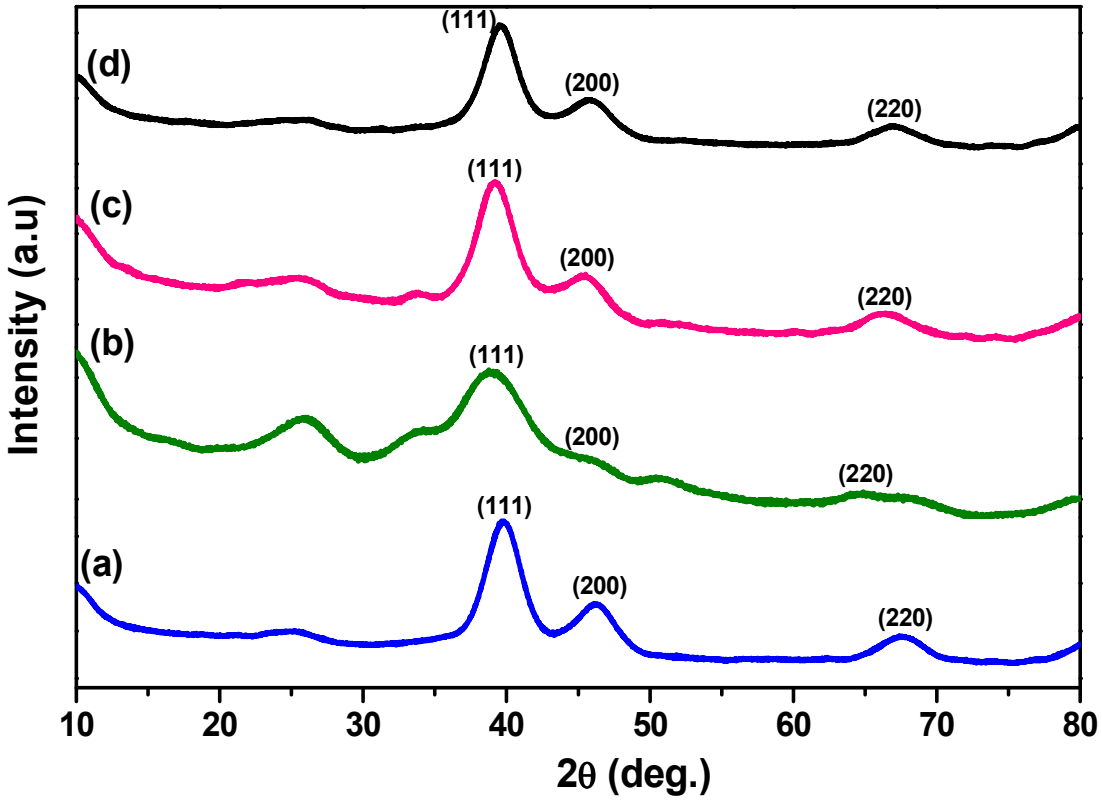

Fig. 1

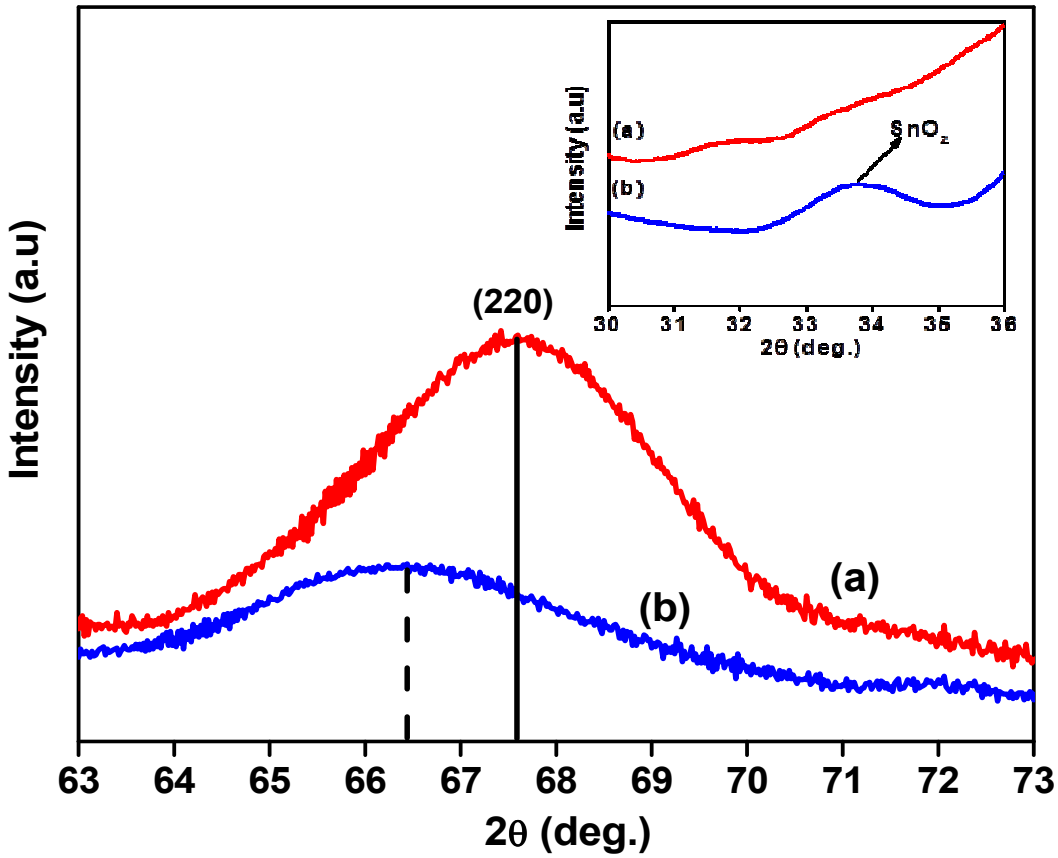

Fig. 2

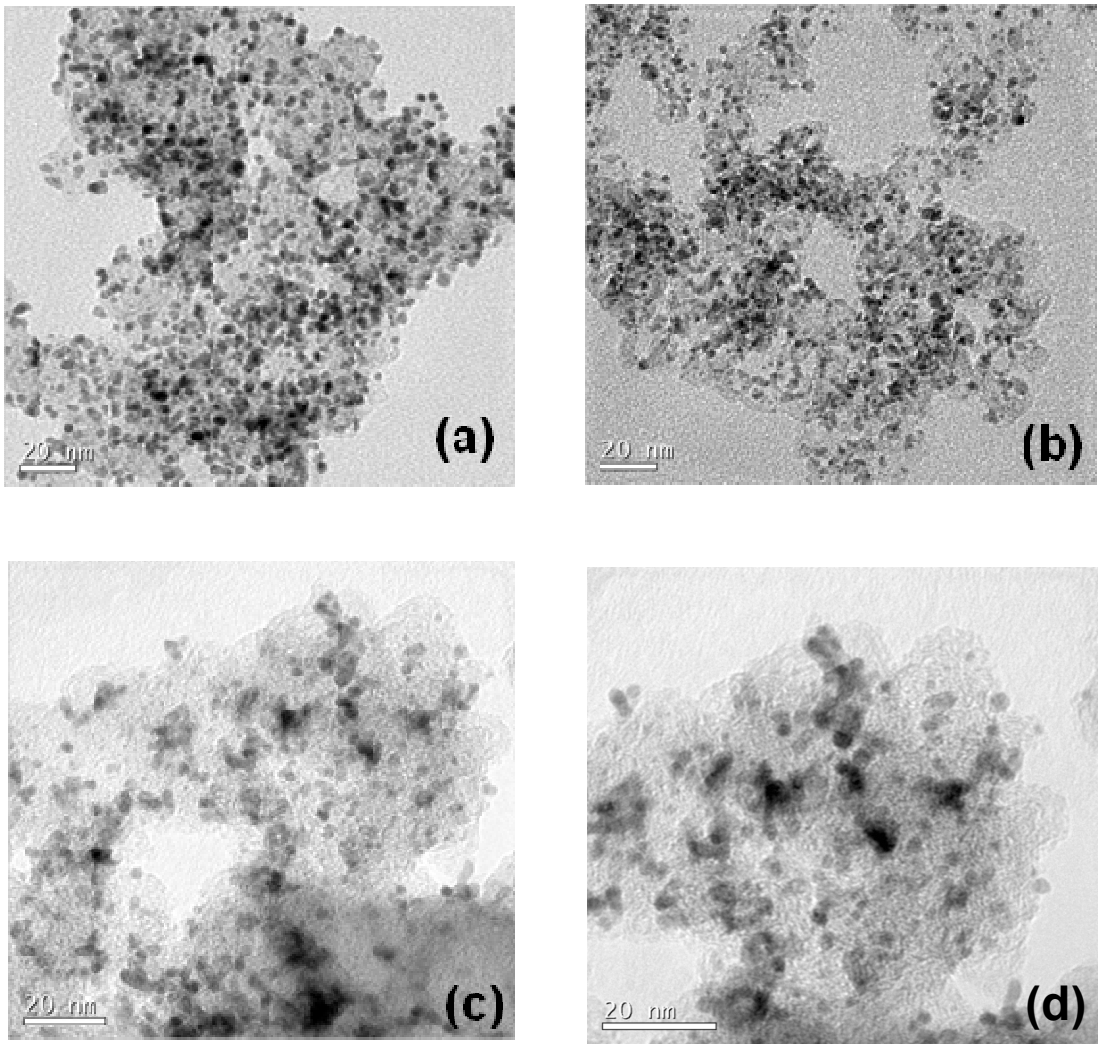

Fig. 3

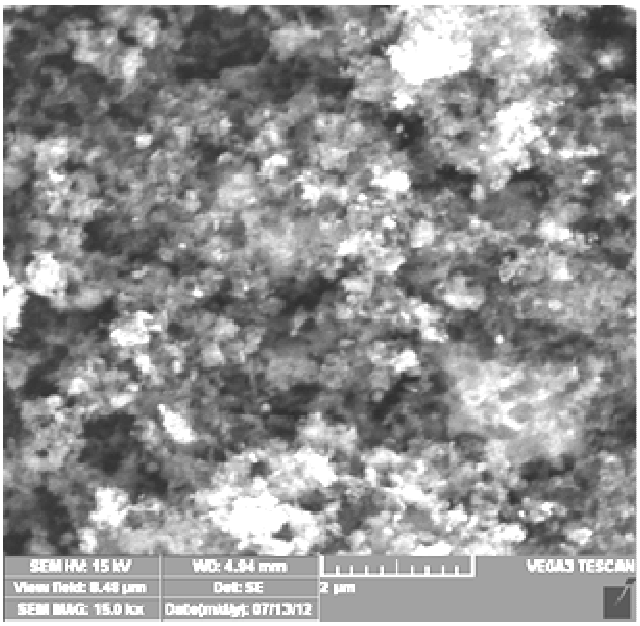

(a)

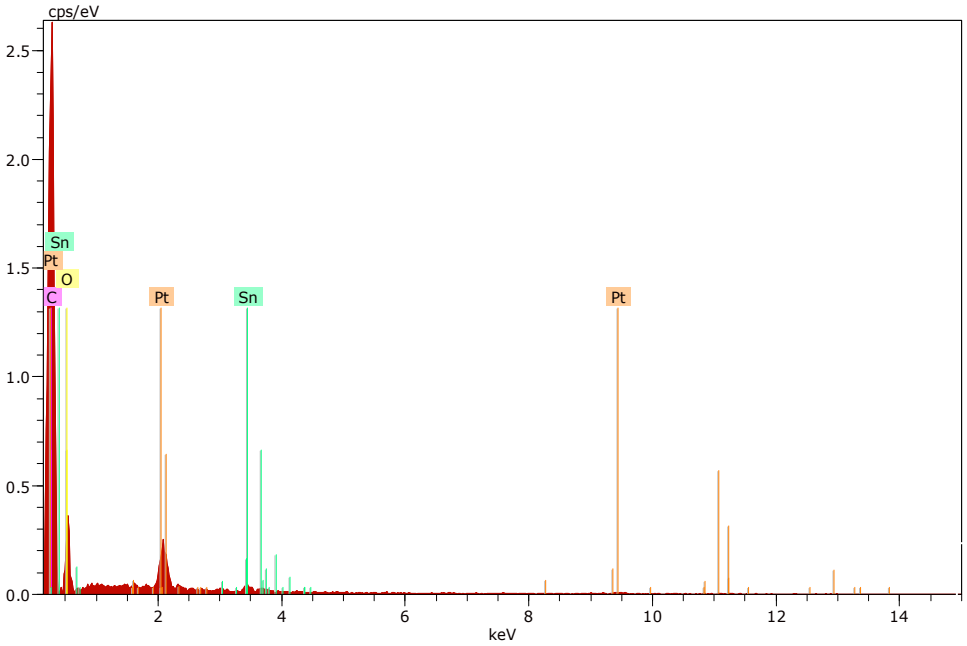

(b)

Fig. 4

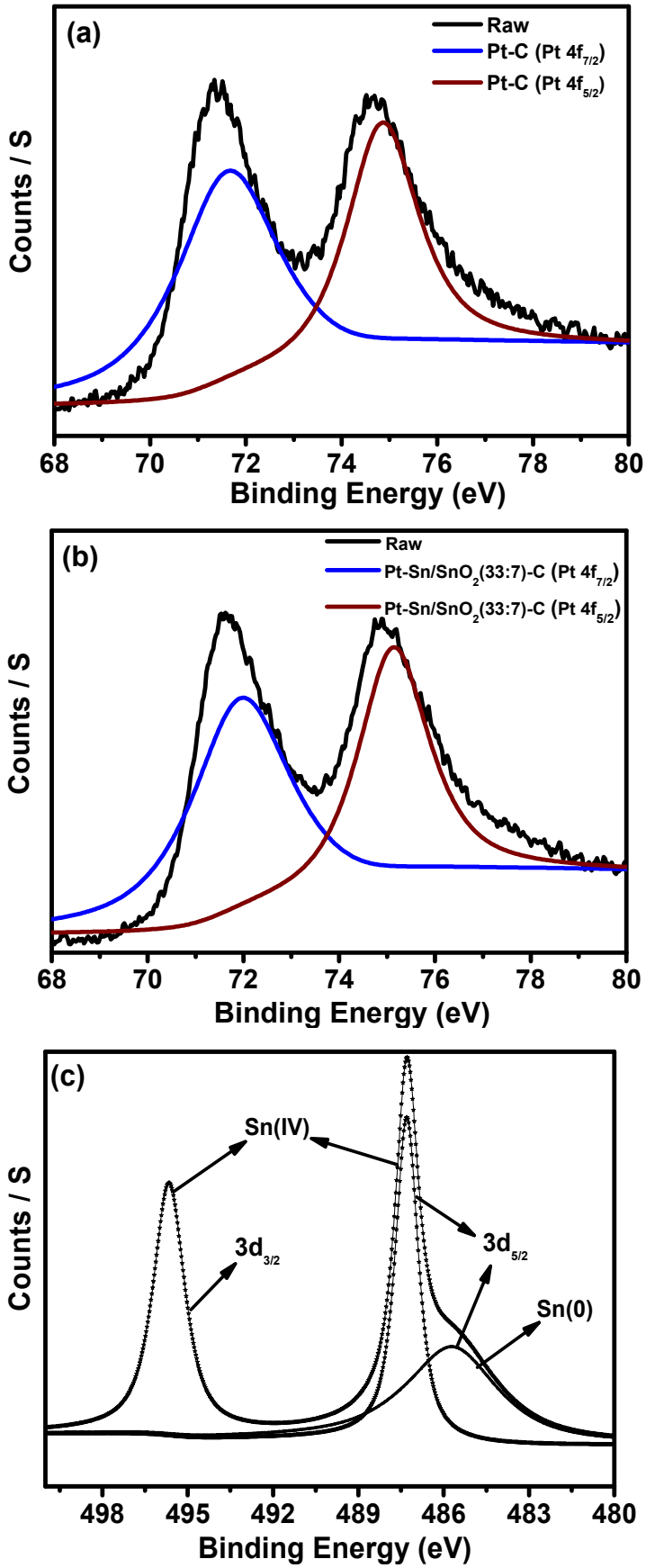

Fig. 5

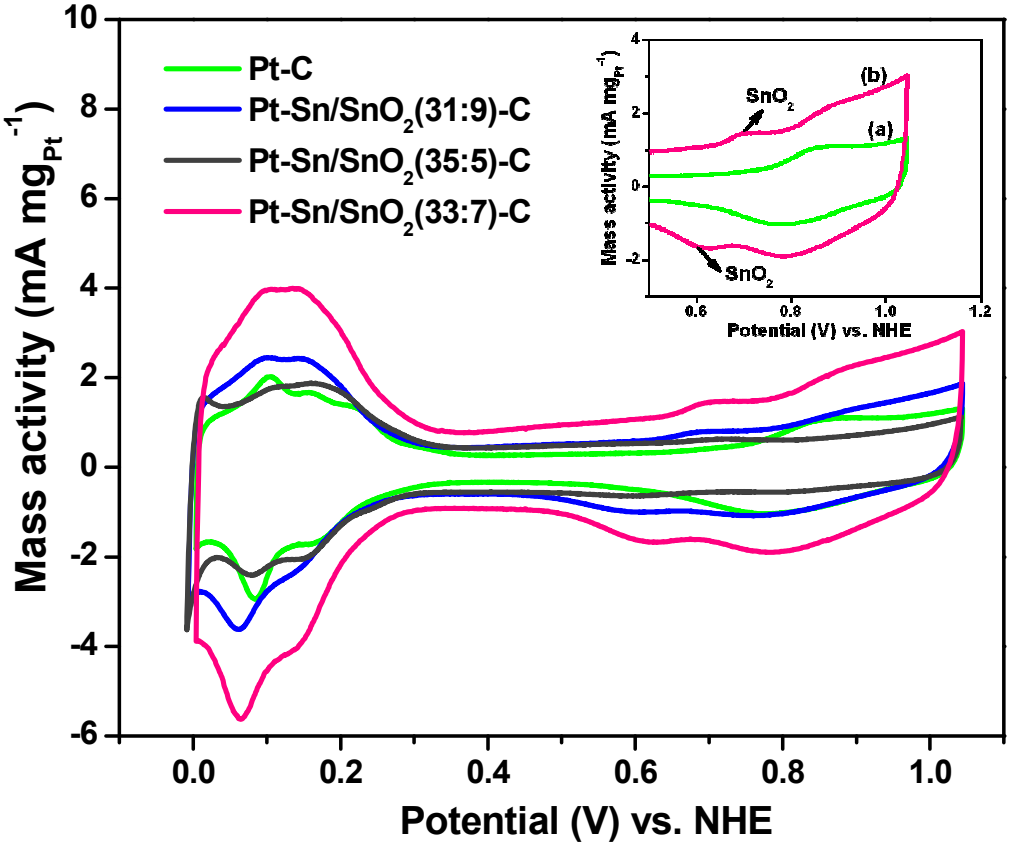

Fig. 6

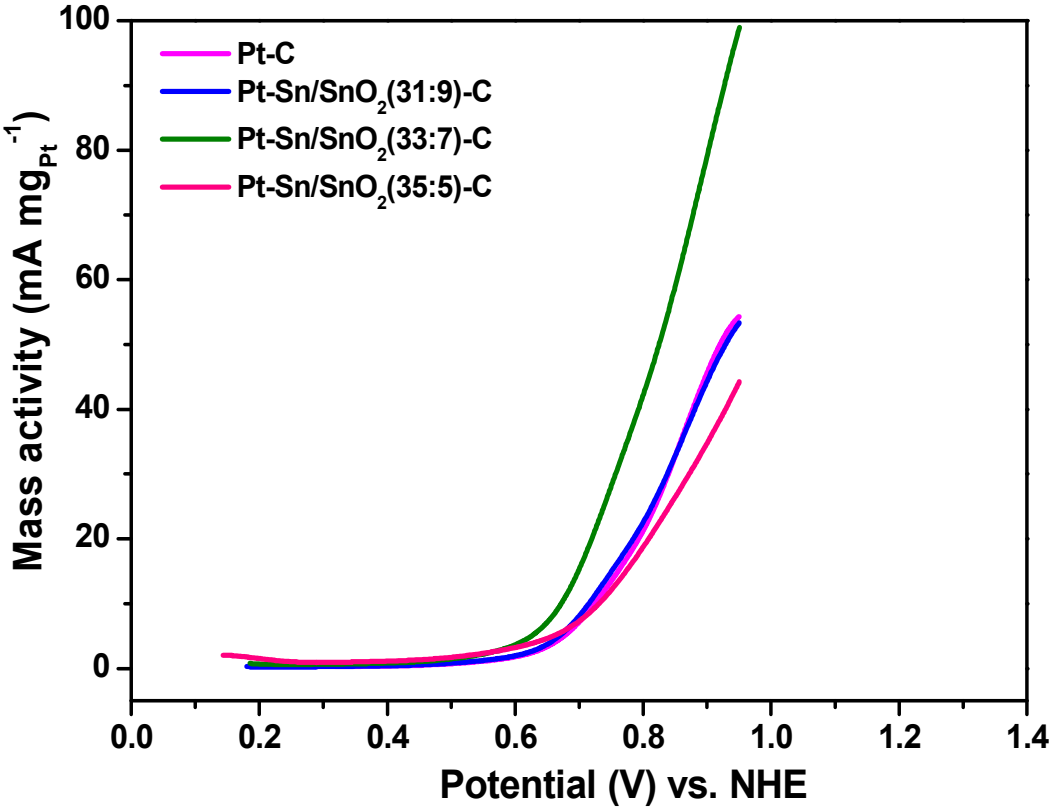

Fig. 7

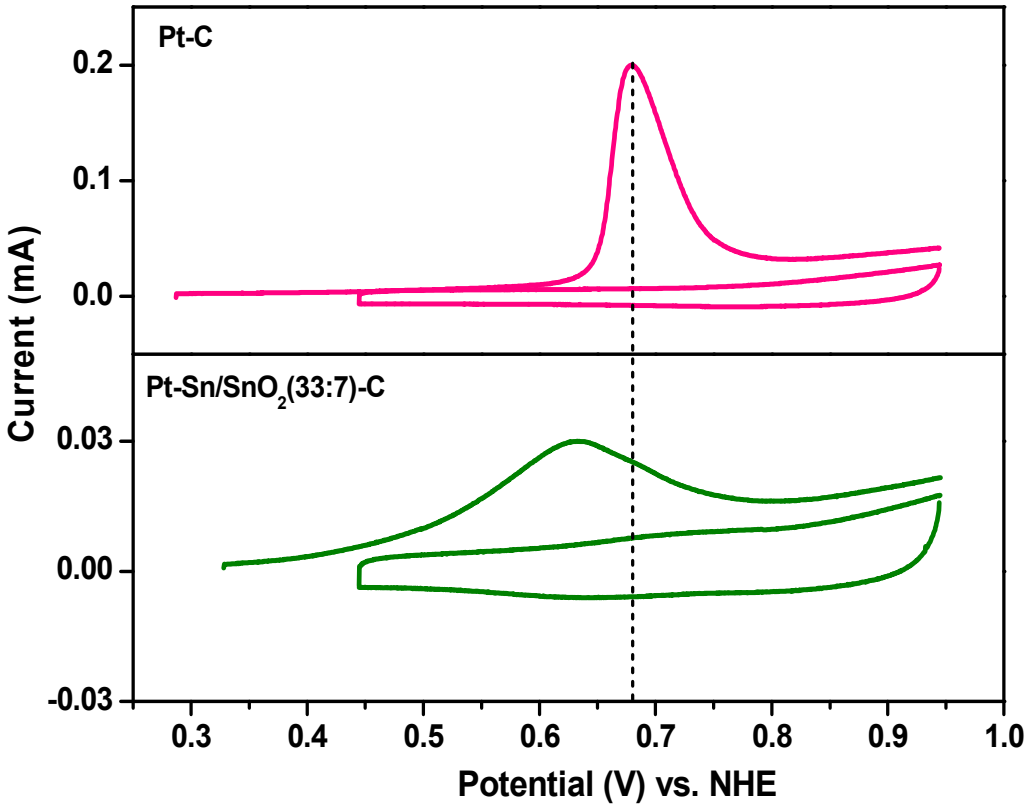

Fig. 8

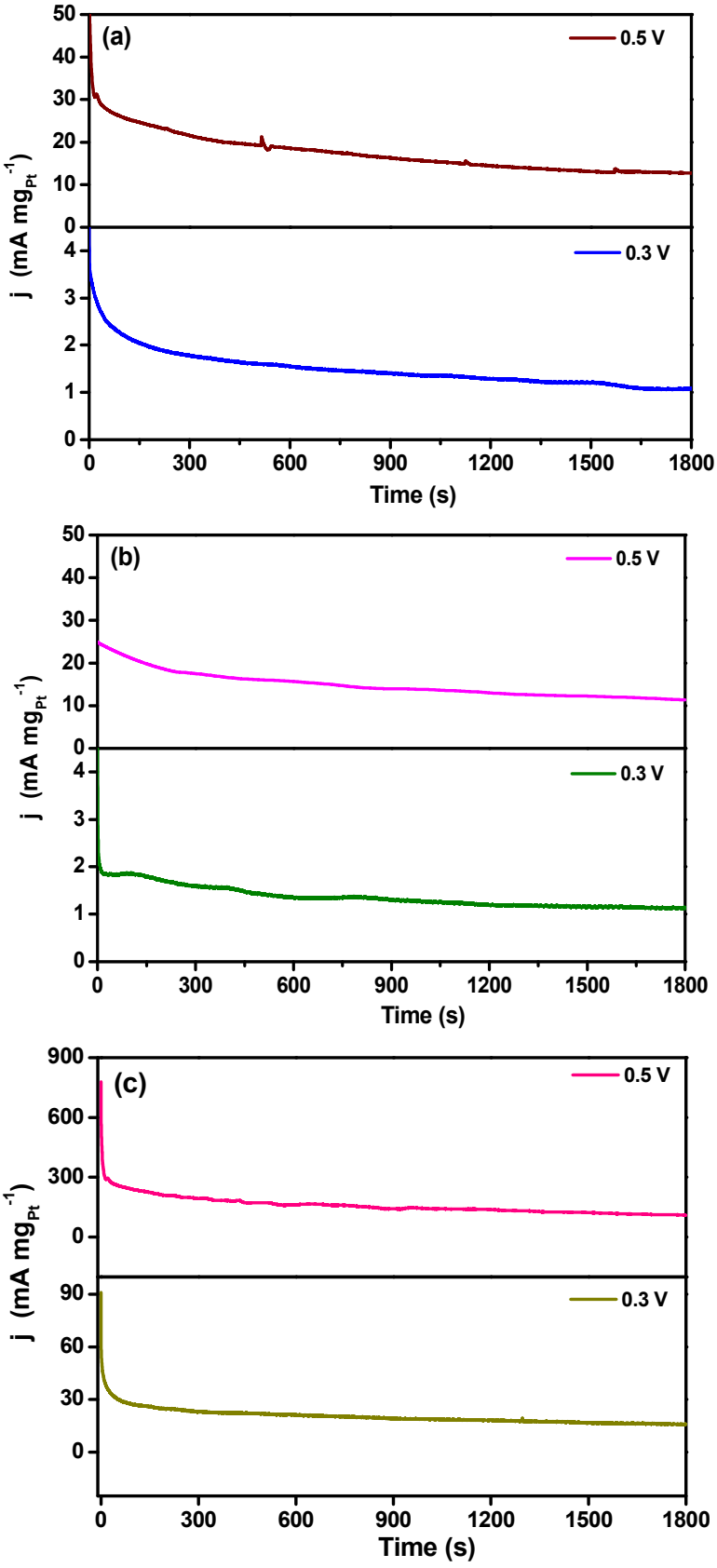

Fig. 9

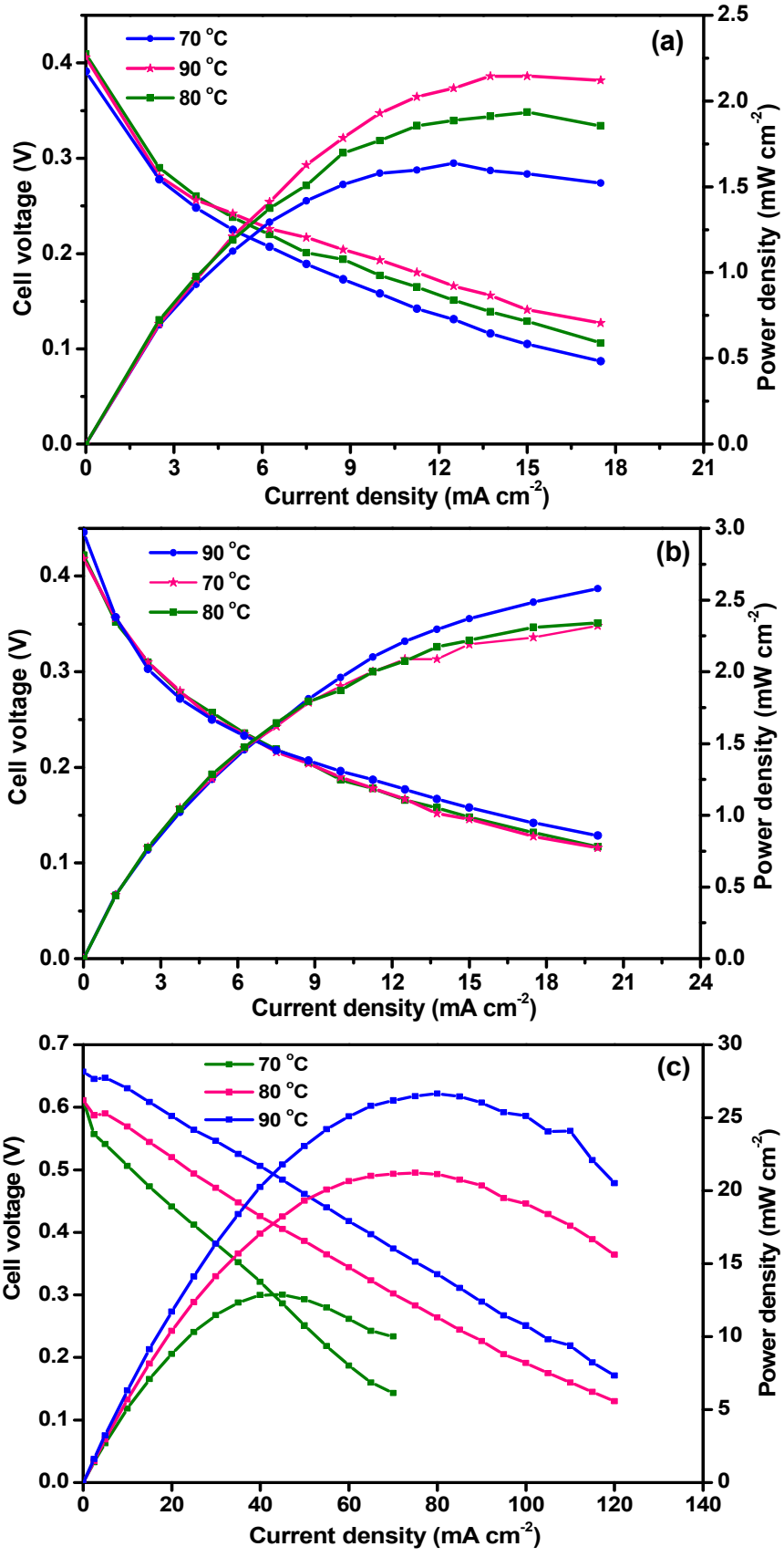

Fig. 10

Table 1

Physical parameters of the catalysts

Catalyst	Crystallite size (nm)	TEM particle size (nm)	Pt to Sn atomic ratio in ICP-OES (%)
Pt-C	4.5	3.0 - 3.5	-
Pt-Sn/SnO_2(31:9)-C	3.9	1.5 - 2.0	30.63 : 8.69
Pt-Sn/SnO_2(33:7)-C	4.2	2.0 - 2.5	32.85 : 6.79
Pt-Sn/SnO_2(35:5)-C	4.4	2.5 - 3.0	34.58 : 4.87

Table 2

Electrochemical parameters of the catalysts

Catalyst	Electrochemical surface area ($m^2\ g^{-1}$)	Mass activity $I_{0.8\ V}$ ($mA\ mg^{-1}_{pt}$)
Pt-C	56	21
Pt-Sn/SnO_2(31:9)-C	72	23
Pt-Sn/SnO_2(33:7)-C	115	42
Pt-Sn/SnO_2(35:5)-C	62	19

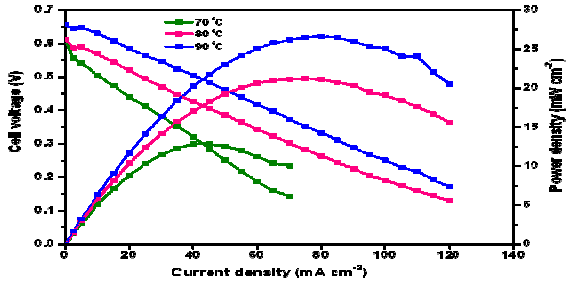

Steady-state performance data of DEFCs (CH_3CH_2OH and O_2) comprising MEA containing Pt-Sn/SnO_2(33:7)-C anode catalyst prepared using decal transfer method.